Journal of Power Sources 247 (2014) 587–593

Contents lists available at ScienceDirect

Journal of Power Sources

journal homepage: www.elsevier.com/locate/jpowsour

Effect of the co-spun anode functional layer on the performance of the direct-methane microtubular solid oxide fuel cells

Xiuxia Meng [a, b], Xun Gong [b], Yimei Yin [a], Naitao Yang [b, *], Xiaoyao Tan [b, c], Zi-Feng Ma [a, *]

[a] Institute of Electrochemical and Energy Technology, Department of Chemical Engineering, Shanghai Jiao Tong University, Shanghai 200240, China
[b] School of Chemical Engineering, Shandong University of Technology, Zibo 255049, China
[c] Department of Chemical Engineering, Tianjin Polytechnic University, Tianjin 300387, China

HIGHLIGHTS

- Dual-layer NiO–YSZ/p-YSZ hollow fibers were co-spun through phase-inversion process.
- MT-SOFCs with controllable AFLs were fabricated based on the dual-layer microtubes.
- A prepared MT-SOFC fueled with CH_4 was stably operated for 85 h.

ARTICLE INFO

Article history:
Received 15 June 2013
Received in revised form
23 August 2013
Accepted 26 August 2013
Available online 11 September 2013

Keywords:
Micro tubular solid oxide fuel cell
Dual-layer hollow fiber
Anode functional layer
Carbon-resistance
Co-spinning-sintering

ABSTRACT

NiO–YSZ/porous YSZ (NiO–YSZ/p-YSZ) dual-layer hollow fibers have been fabricated by a co-spinning-sintering method, on which a dense YSZ films has been formed by a dip-coating and sintering process. A LSM–YSZ ink has been dip-coated on the dense YSZ films as cathode, while the Cu–CeO_2 carbon-resistant catalyst has been impregnated in the p-YSZ layer to form double-anode supported micro tubular fuel cells (MT-SOFCs). The thickness of the Ni-YSZ layer, so called anode functional layer (AFL), is controlled from 74 μm to 13 μm by varying the spinning rates of the NiO–YSZ dopes. The maximum power density of an MT-SOFC, which is fabricated based on a thin co-spun AFL, reaches 566 mW cm^{-2} operated at 850 °C fed with dry methane, and is stably operated for 85 h without power declination.

1. Introduction

Micro-tubular solid oxide fuel cells (MT-SOFCs) have attracted increasing interest in recent years because of their unique characteristics such as high volumetric power density, high mass-transfer and heat-transfer efficiency and rapid start-up/shut-down operation [1–3]. Nickel-based cermet has been widely applied as the anode of MT-SOFCs due to its high electrochemical activity to hydrogen or hydrocarbons. However, carbon may deposit on the nickel catalyst when the cell is fed with hydrocarbon fuels, leading to a quick degradation of the fuel cell performance [4].

A double anode including a functional layer and an electronic conducting layer has been proposed to resist carbon deposition [5]. For example, the Cu–CeO_2 catalyst layer over Ni–YSZ layer has shown good performance for the direct utilization of hydrocarbons in SOFC [6]. Since the poor combination between the Cu–CeO_2 and Ni–YSZ layers poses critical issues of the stability and function of the composite structure, a Ni–CeO_2 interlayer is suggested to be sandwiched between the two layers [7]. However, a thicker anode might lead to a more significant resistance because less fuel reaches to the interface between the anode and the electrolyte. To reduce the voltage loss, a graded double anode, which consists of a macroporous support layer and a microporous anode functional layer (AFL), has been suggested for the preparation of SOFCs [8]. The microporous AFL increases the length of the TPB, resulting in faster kinetics of the electrochemistry reactions. Furthermore, the macroporous support is beneficial for a rapid diffusion of fuels and products, leading to a lower concentration polarization. Because AFL poses low electronic conductivity and high diffusion resistance, it is generally prepared to a very thin layer for both maximizing anode TPB length and restraining the activation polarization [9,10].

* Corresponding authors. Tel.: +86 21 54742894; fax: +86 21 54747717.
E-mail addresses: naitaoyang@126.com (N. Yang), zfma@sjtu.edu.cn (Z.-F. Ma).

0378-7753/$ – see front matter © 2013 Elsevier B.V. All rights reserved.
http://dx.doi.org/10.1016/j.jpowsour.2013.08.133

Preparations of AFL are generally achieved by the in-situ layer-by-layer deposition technique such as dry-pressing [9,11], dip-coating [12], tape casting [13] and spray coating [10] methods. It is fairly time-consuming and laborious, and may lead to cracks on the interfaces and peeling off between different layers. Furthermore, the layer-by-layer deposition is quite difficult to construct a thin AFL in such a tiny structure of MT-SOFCs. In this work, a novel Ni–YSZ/porous YSZ (NiO–YSZ/p-YSZ) dual-layer hollow fiber structure developed by a co-spinning-sintering process based on the phase inversion technique [14–17] is applied to fabricate a compact double anode in one step. Such dual-layer hollow fibers are designed to consist of a microporous AFL layer and a macroporous substrate so as to impregnate Cu–CeO_2 carbon-resistant catalysts. The study will mainly focus on the effect of the AFL on the performances of the double-anode supported MT-SOFCs with dry methane as the fuel.

2. Experimental

2.1. Materials

Commercially available yttria-stabilized zirconia (YSZ) powder with purity of 99.9% and particle size of 20–30 nm (Yitong Co. Ltd., Weifang, China) was used as the electrolyte material. The cathode material, $La_{0.8}Sr_{0.2}MnO_{3-\alpha}$ (LSM) was synthesized via the Pechini method. NiO (AR grade, Sinopharm Chemical Reagent Co., Ltd.) was used as the anode material. Polyethersulfone (PESf, Radel A-300, Ameco Performance, USA), *N*-methyl-2-pyrrolidone (NMP, >99.8%, Kermel Chem Inc., Tianjin, China) and spherical graphite (20–30 μm in diameter, Hengchang Graphite Co. Ltd., Chenzhou, China) were used as the polymer binder, solvent and pore former, respectively, for the preparation of the spinning dopes. Deionized water was used as the internal and external coagulants.

2.2. Preparation of Ni–YSZ/p-YSZ dual-layer hollow fibers

The dual layer NiO–YSZ/p-YSZ hollow fiber was prepared by a co-spinning-sintering process based on the phase inversion method. A calculated amount of PESf pellets was dissolved in NMP in a 125 cm^3 wide-neck bottle to form a polymer solution. YSZ (mixed with 20 wt % of graphite) or NiO–YSZ (6:4 in weight ratio) powders, which had been dried at 120 °C for 12 h in advance, were added gradually into the PESf-NMP polymer solution under stirring. The stirring was carried out continuously for 48 h to ensure that all the powders were dispersed uniformly in the polymer solution. Physica UDS-200 rheometer was used to measure the viscosity of the dopes at room temperature prior to the spinning. The parameters of the spinning dopes are listed in Table 1.

After degassing at room temperature for 2 h, the NiO–YSZ and p-YSZ dopes were transferred separately to two stainless steel syringes. With the help of three syringe pumps (LSP01-1BH, Longer Precision Pump Co., Ltd., Baoding, China), the two dopes and the internal coagulant were pressed simultaneously through a triple-orifice spinneret, passing through a 10 cm air gap, into a water coagulant bath. To control the thickness of anode functional layers (AFLs), the spinning rates of the NiO–YSZ outer dopes were set at 1, 2 and 4 mL min^{-1} (marked with anode-1, anode-2 and anode-4, respectively). The flow rates of p-YSZ dope and the internal coagulant were set at 10 mL min^{-1} and 14 mL min^{-1}, respectively. The co-spun hollow fibers were immerged in the external coagulation bath to complete the solidification process. After 24 h, the dual-layer hollow fiber precursors were taken out from the water bath, cut into pieces of 20 cm in length, straightened and dried at room temperature successively. Then the precursors were sintered at 1450 °C for 4 h to form NiO–YSZ/p-YSZ dual-layer hollow fibers. Ni–YSZ/p-YSZ hollow fibers were obtained by reducing in hydrogen at 700 °C for 2 h.

Table 1
Spinning parameters for dual-layer NiO–YSZ/p-YSZ hollow fibers.

Spinning dope	Spinning rate (mL min^{-1})	Mass (wt%)					Viscosity (mPa s)
		NiO	YSZ	PESf	NMP	Graphite	
Anode-1	1	37.7	25.1	8	29.2	/	6500
Anode-2	2	37.7	25.1	8	29.2	/	6500
Anode-4	4	37.7	25.1	8	29.2	/	6500
p-YSZ dope	10	/	45.71	9.52	33.33	11.42	53800

2.3. Fabricating and testing of MT-SOFCs

A dense YSZ electrolyte membrane was firstly dip-coated on the outer surface of dual-layer NiO–YSZ/p-YSZ hollow fiber precursors and sintered at 1450 °C for 4 h, and then, the cathode ink was dip-coated on the sintered YSZ membrane and fired at 1050 °C for 2 h. After calcining the cathode, CuO–CeO_2 mixture (3:1 in weigh ratio) was loaded inside the p-YSZ framework by infiltration of a mixing solution containing $Cu(NO_3)_2$ and $Ce(NO_3)_3$ in ethylene glycol (30 wt%), then was calcined at 450 °C for 1 h. The impregnation procedures were repeated for three times, increasing the weight of the cells for about 10%.

To test the fuel cell performance, one silver wire was wrapped around the outer side, and another was looped inside the fiber lumen as the current collectors. Silver paste, diluted by ethanol, was coated by flushing and brushing on the anode and cathode surfaces, respectively. Conductive Ag paste was used to stick the silver wires onto the electrode surfaces. The fuel cell with current collectors fixed both ends on two small quartz tubes with an inorganic sealant was housed in a large quartz tube, as shown in Fig. 1. A K-type thermocouple was used to monitor the operation temperature. Before the measurement, the anode was reduced by flowing hydrogen on the shell side at 700 °C for 2 h. *I–V* & *I–P* data of the cells were collected using a DC Electronic Load (Keithley 2440-5A) at 700–850 °C using methane as the fuel and air as the oxidant. The flow rates of methane and air were fixed at 40 and 90 mL min^{-1}, respectively. The stability of the cell was tested using a DC Electronic Load under a voltage of 0.7 V. Electrochemistry Resistance Spectrum (EIS) of the cell under open circuit were measured by an electrochemistry workstation (Zahner IM6ex, Germany) in the ranging of frequency from 1 M to 0.01 Hz with amplitude of 10 mV.

2.4. Characterizations

Microstructures of the hollow fibers were ascertained by field emission scanning electron microscopy (FESEM, FEI Sirion 200, the Netherlands). Gold sputter coating was performed on the samples before the measurements. The elemental line distributions of the samples were investigated by the Energy Dispersive X-ray (EDX).

3. Results and discussions

3.1. Microstructure of dual-layer hollow fiber membranes

The external diameters of the prepared dual-layer hollow fibers are about 1.5 mm. Fig. 2 shows the microstructure of the reduced dual-layer hollow fibers. The interfaces between Ni–YSZ and p-YSZ are tightly combined without any gaps or peeling off (Fig. 2(b1–b3)). Variation in AFL thickness of the dual-layer hollow fibers has been achieved by simply adjusting the extrusion rate. Fig. 2(b1–b3) also shows that the spinning rates of the NiO-YSZ

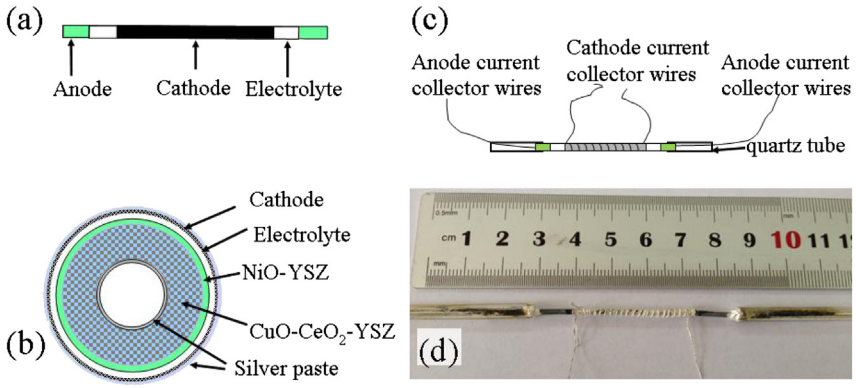

Fig. 1. Microtubular SOFC configuration: (a) schematic diagram of Microtubular SOFC, (b) cross-section of the unit cell coated with silver, (c) completed test cell, and (d) the photograph of assembled MT-SOFC.

dopes affect the thicknesses of the AFLs significantly, which vary from 74, 25 to 13 μm when the spinning rates are controlled from 4, 2 to 1 mL min^{-1}, as well as the AFLs are uniformly covering around the support tubes. Observed from Fig. 2, the two layers pose different pore structures, shown as macro pores in the supports due to addition of pore former and micro pores in the AFLs resulting from the reduction of NiO to Ni. The internal surfaces of the hollow fibers also show porous microstructures (Fig. 2(d1–d3)), which is benefit for impregnating of carbon-resistant catalyst into the p-YSZ substrate.

3.2. Microstructure of the MT-SOFCs

Fig. 3 shows the SEM and EDX of the prepared MT-SOFCs based on the double anode. The magnified part of the cross section in Fig. 3(a1 and a3) clearly displays four different layers (marked by white lines) in a sequence of cathode/electrolyte/Ni–YSZ/Cu–CeO_2–YSZ. The interfaces of LSM/YSZ and YSZ/AFL are very clear because the cathode and electrolyte layers are prepared through dip-coating processes. Gaps or defects sometimes are formed at the boundaries (Fig. 3(b3)). Nevertheless, the interfaces between the AFLs and the supports are compacted tightly, difficult to discriminate their boundaries (Fig. 3(a1–c1)). The prerequisite of such achievement is the successful preparation of a high quality of NiO–YSZ/p-YSZ dual-layer hollow fiber, which was prepared by co-spinning in one procedure. The two co-spinning dopes are flowing liquids when they are pressed out from the spinneret, mixing a little before immerging into the coagulant. Therefore these interfaces after co-sintering are highly integrated, thermally matched, and mechanically compatible, almost zero defect at these boundaries, consistent with the other dual-layer hollow fibers, such as YSZ/Ni–YSZ and YSZ/LSM–YSZ [18,19].

EDX graphs (Fig. 3(a2–c2)) show that most of Cu and Ce elements are impregnated into the nickel free p-YSZ layer, and only little amount of Cu penetrates into Ni–YSZ layer. A continuous Cu deposition is helpful in obtaining a good electrically conducting network. For example, Fig. 3(a2) shows EDX graphs of line distribution for Ni(red), Cu(green) and Ce(blue) of the MT-SOFCs supported by Ni–YSZ/Cu–CeO_2–YSZ double anode. In this picture, Ni is intensively located at the AFL and has hardly been affected by the followed processes of cathode-sintering and Cu–CeO_2 impregnating. The distribution line of Cu is mainly located on the support

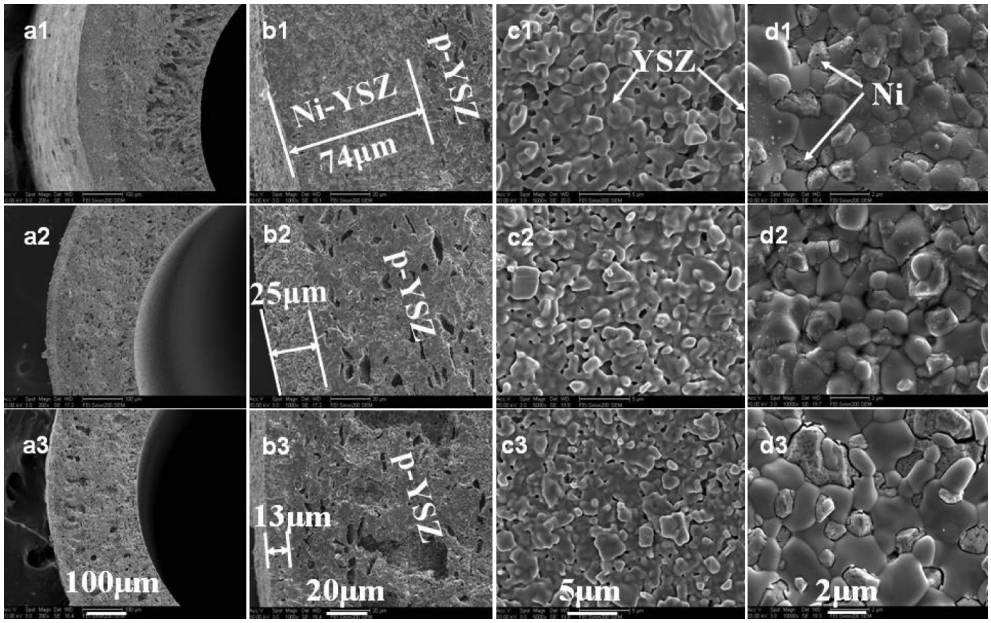

Fig. 2. Microstructure of Ni–YSZ/p-YSZ dual-layer hollow fibers with the spinning rate of NiO–YSZ dopes from 4 mL min^{-1} (1), 2 mL min^{-1} (2), to 1 mL min^{-1} (3). (a) Cross section, (b) magnified anode functional layer, (c) inner surface and (d) outer surface.

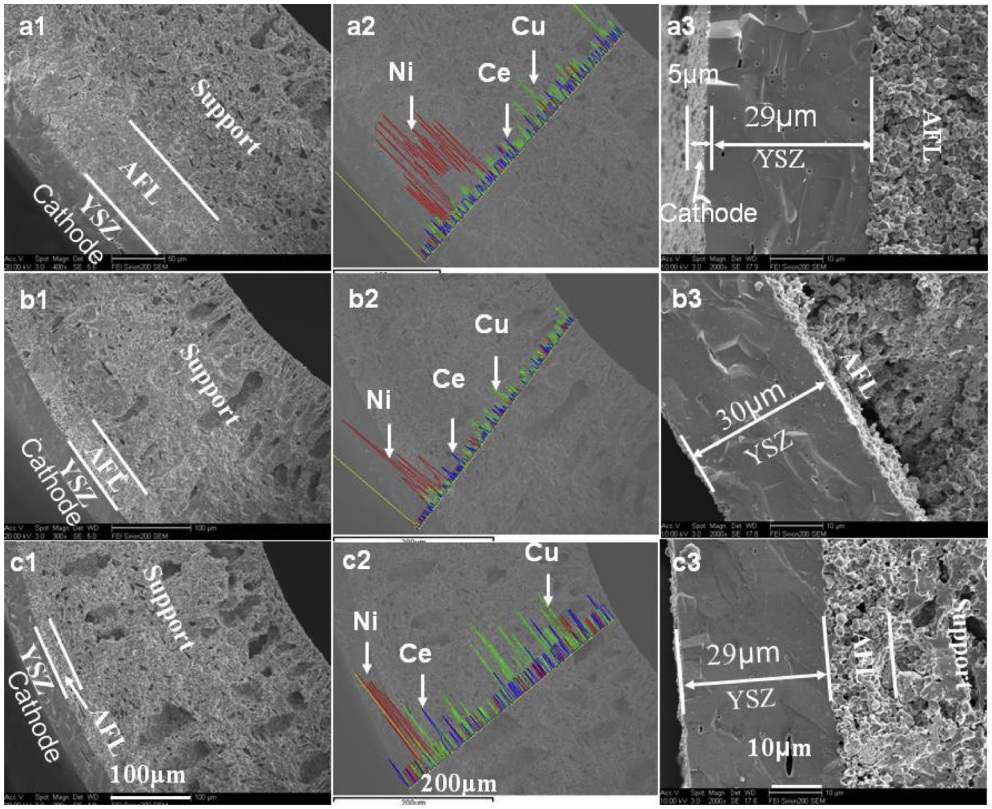

Fig. 3. SEM and EDS of MT-SOFCs supported by dual-composition anode. (a) Anode-4; (b) anode-2; (c) anode-1. (1)cross-section; (2) line distribution of Ni(red), Cu(green) and Ce (blue); (3) microstructure of YSZ/AFL area. (For interpretation of the references to color in this figure legend, the reader is referred to the web version of this article.)

layer but is also found in AFL. The successful penetration of Cu and Ni–Cu contact are beneficial for prompt removing of the electrons in the electrochemical oxidation site, leading to lower ohmic resistance and higher cell performance [20].

Fig. 4 shows the morphology of $CuO–CeO_2$ impregnation into the p-YSZ support layer. From Fig. 4(a2), the $CuO–CeO_2$ particles are homogenously distributed inside the p-YSZ framework, indicating a continuous network for electrical conducting and a large surface

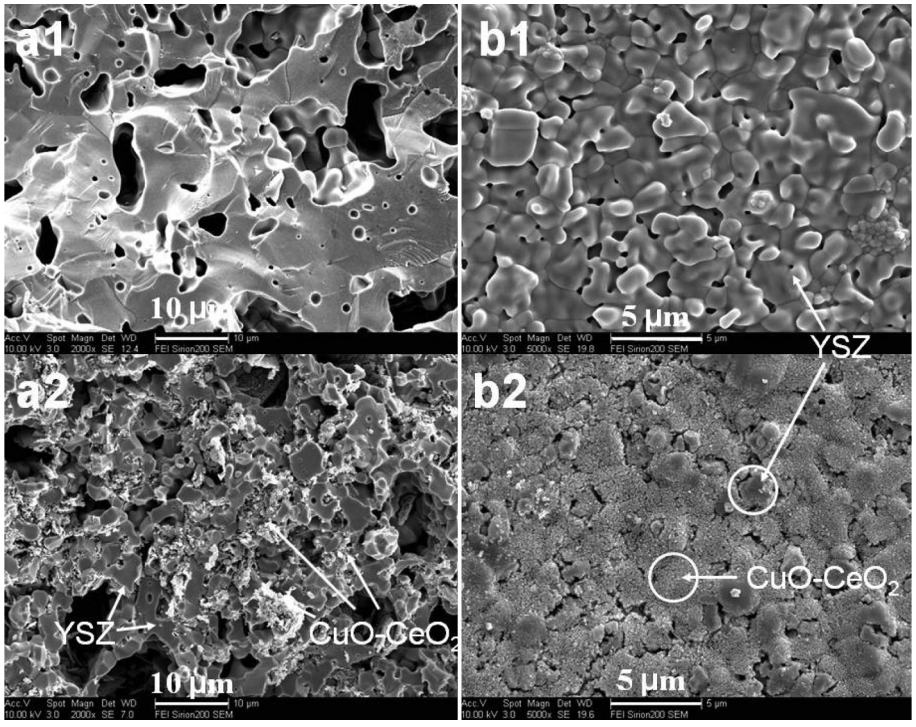

Fig. 4. Microstructure of the p-YSZ support (1) before and (2) after $CuO–CeO_2$ impregnation. (a) Cross section, (b) inner surface.

area for methane-pyrolysis in the anode support. Although the porosity of cross section and inner surface decreases a lot after impregnation, the anode support still keeps a porous structure (Fig. 4(a2 and b2)). It can be deduced that the support layer will be more porous after reducing by hydrogen, beneficial for both gas diffusion and carbon-resistance using hydrocarbon fuels.

3.3. Performance of the MT-SOFCs with AFL

Fig. 5 shows the initial *I–P* & *I–V* curves of micro-tubular SOFCs supported by the double anode operated at 700–850 °C fueled with CH_4. Considering *I–V* curves, all cells exhibit potential values close to the theoretical open-circuit voltage (OCV), indicating that the electrolyte layer is very dense without short circuit, consistent with Fig. 3. The OCVs increase slightly with the increasing temperatures

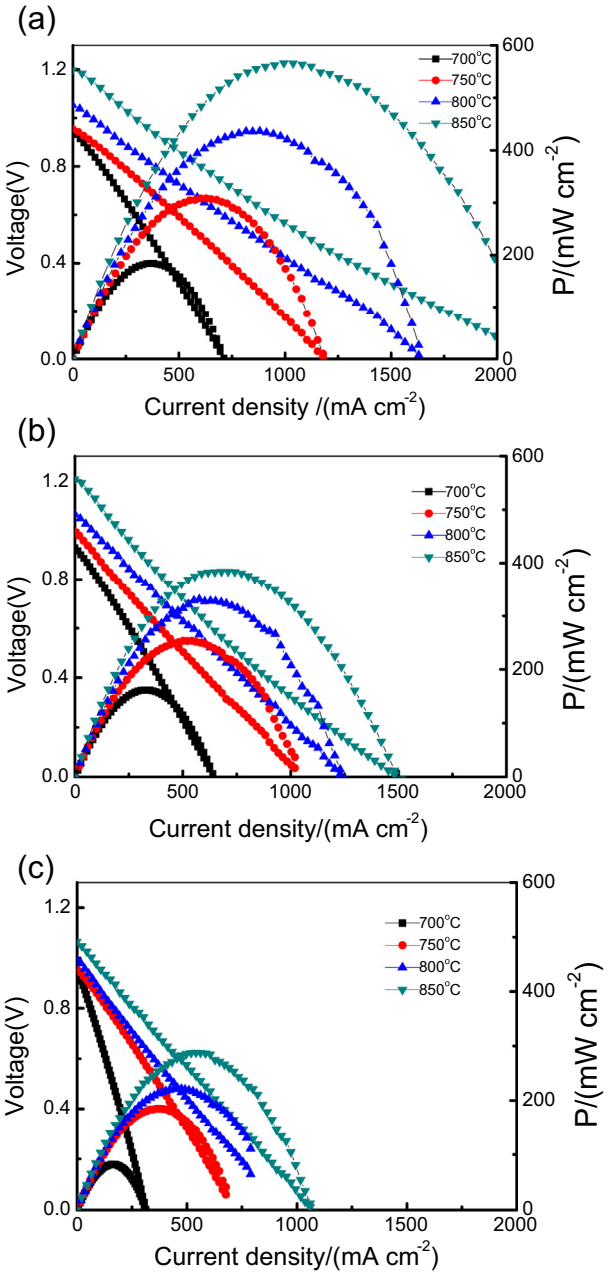

Fig. 5. Performance of MT-SOFCs supported by Cu–CeO_2–YSZ/Ni–YSZ dual layer anode: (a) anode-1, (b) anode-2, (c) anode-4.

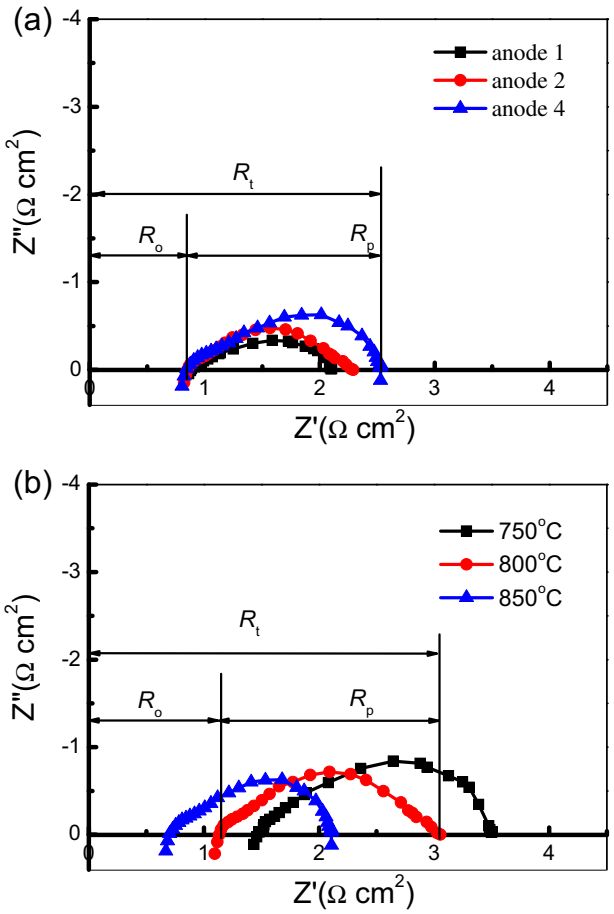

Fig. 6. EIS of MT-SOFCs with Cu–CeO_2–YSZ/Ni–YSZ dual layer anode using methane fuel at open circuit voltage. (a) different anodes operated at 800 °C, (b) anode-1 at different temperatures.

from 700 °C to 850 °C using CH_4 as the fuel, which is consistent with the thermodynamical calculations of SOFC system in the published data [20,21]. The maximum power densities of the cells are 566, 384 and 288 mW cm^{-2} at 850 °C, respective to the cells with anode-1, anode-2 and anode-4. The thinner AFL leads to the lower resistance of gas and ion diffusion, the more rapid kinetics of electrochemistry, and the less anode polarization. Therefore, a thinner AFL may improve the cell performance significantly. The peak power density of the prepared direct-methane SOFC is 436 mW cm^{-2} operated at 800 °C, near to the peak value of a micro

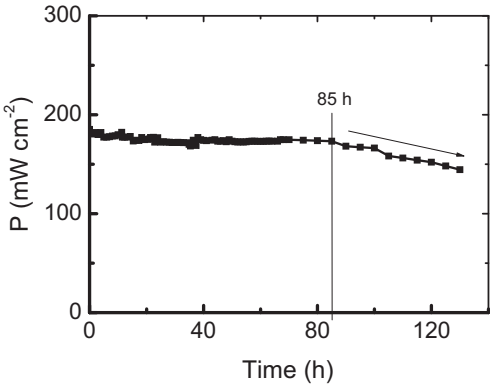

Fig. 7. Long-term stability of MT-SOFC for anode-1.

SOFC fed with pure hydrogen, 485 mW cm^{-2} [19], but much higher than the performance of a cathode-supported MT-SOFC [18], which is only 200 mW cm^{-2}.

Fig. 6 shows EIS of MT-SOFC supported by Ni–YSZ/Cu–CeO_2–YSZ double anode fueled with dry methane. The intercept on the real axis at high frequency represents the ohmic resistance of the cell (R_o), including the resistances of electrolyte, lead wires and contacts [22]. The intercept at low frequency corresponds to the total resistance of the cell (R_t). The difference of intercepts between the high frequency and low frequency on the real axis represents the polarization resistance (R_p) of the cell [23,24]. From Fig. 6(a), R_o vary little because the electrolyte thicknesses and the interfacial contacts are almost the same, while the R_t and R_p increase with the increasing thicknesses of AFLs. Theoretically, The thickness of the area for electrochemical reaction is generally less than 10 μm [25]. Too thin an AFL area cannot supply enough three phase boundaries (TPBs), while too thick of it leads to higher resistance. Therefore, an appropriate AFL thickness is beneficial for enhancing the power output of the cell, consistent with Fig. 5.

In Fig. 6(b), R_t, R_o and R_p decrease with the increasing of operation temperature, due to the enhanced ionic conductivity of the electrolyte and accelerated electrode kinetics. R_o decreases from 1.49, 1.13 to 0.71 Ω cm^2 and R_p decreases from 2.03, 1.89 to 1.39 Ω cm^2 with the increasing temperature from 750, 800 to 850 °C. These values indicate that both R_o and R_p dominate the total cell resistance. Therefore, besides thinning the electrolyte membrane, the cell performance can be further improved by optimizing the anode microstructure.

3.4. Stability of MT-SOFCs fueled with CH_4

Fig. 7 shows the power density of MT-SOFC with anode-1 as a function of time operated at 800 °C and 0.7 V fed with methane. After the initial electrode activation, the output of the cell reaches to 180 mW cm^{-2}. After a stable operation for 85 h, the power density slowly declines to 145 mW cm^{-2} in the next 45 h. The declination trend can be ascribed to the slow carbon deposition in AFL, since the low declination slope implies a slow rate of catalyst degradation. However, the prepared cell based on Ni–YSZ/Cu–CeO_2–YSZ double anode still keeps a longer stable time than traditional direct-methane SOFCs with Ni/YSZ anode [20,26–28]. This improvement should be resulted in the resistance of C–C bond formation in Cu–CeO_2 catalyst [29]. POM reaction takes place firstly on the Cu–CeO_2–YSZ support [30,31] without carbon deposition (Fig. 8(c)). Then the generated syngas and little methane diffuse to AFL to perform the electrochemical reaction. Thin AFL is a region of oxygen enrichment, adjoining to the electrolyte, leading to much rapid rate of oxidation reaction than coke formation [32]. Even if the coke is formed in this region after the first 85 h (Fig. 8(b)), it is also electrically conductive carbonaceous material on the anode, available for current collection [33], weakening little to the cell performance. Therefore the cell output declines not so fast at the second stage. In addition, the smooth transition from large pore side (p-YSZ) to micro pore side (Ni–YSZ) is also beneficial for improving the cell performance and stabilizing the cell structure, due to their high compatibility based on co-spinning-sintering technology. Even after a long-term operation, the boundary structure is still stable without peeling off or cracks, clearly observed from the SEM pictures (Fig. 8(d)).

Though the performance of a direct-methane fuel cell keeps stable for 85 h, its ohmic resistance and polarization resistance still increase with the time passing, as shown in Fig. 9. The increased polarization resistance implies a little degradation of the cell. Because the coking reaction still performs in Ni–YSZ layer, carbon formation is still inevitable over long time operation, causing irrevocable electrode degradation. However, compared to the traditional direct-methane SOFC with Ni/YSZ anode [20,26–28],

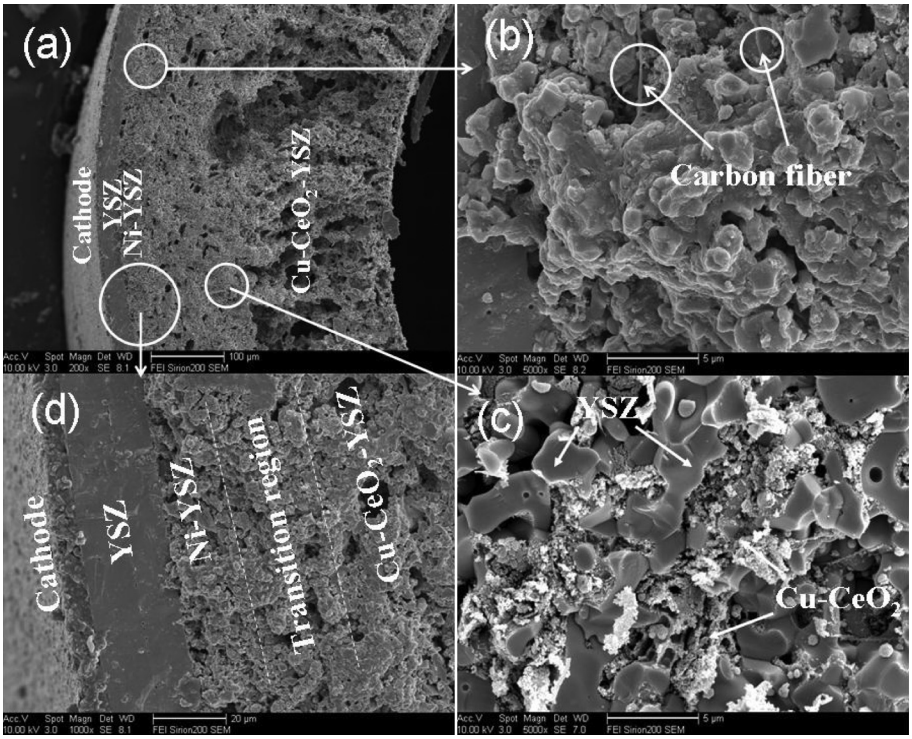

Fig. 8. Carbon morphology of a direct-methane MT-SOFC after long-term test. (a) Cross-section, (b) Ni–YSZ layer (anode-1), (c) Cu–CeO_2–YSZ layer, and (d) the transition region between Ni–YSZ layer.

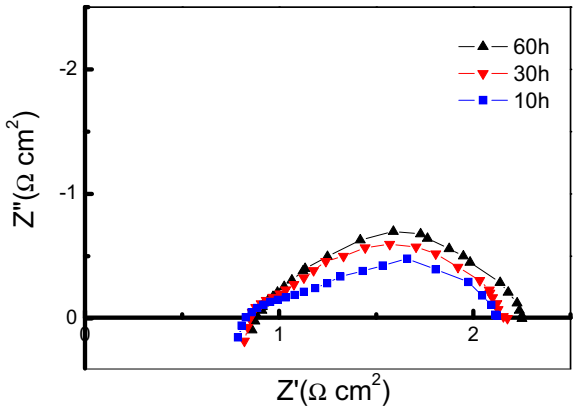

Fig. 9. EIS of the MT-SOFC supported by anode-1 fueled with methane at 800 °C during the long-term test.

the prepared MT-SOFC with the Ni–YSZ/Cu–CeO_2–YSZ double anode shows favorably improved stability.

4. Conclusions

A co-spinning-sintering process was applied to produce NiO–YSZ/porous YSZ (NiO–YSZ/p-YSZ) dual-layer hollow fibers, with which the double-anode supported LSM/YSZ/Ni–YSZ/Cu–CeO_2–YSZ MT-SOFCs have been fabricated. The thickness of the anode functional layer can be controlled from 74 μm to 13 μm by adjusting the spinning rates of the NiO–YSZ dopes. The MT-SOFC with a 13 μm Ni–YSZ layer has shown the maximum power density of 566 mW cm^{-2} at 850 °C using methane as fuel and air as the oxidant, but the output decreases as the AFL thickness increases. Besides, the double-anode supported MT-SOFCs has also exhibited excellent stability against carbon deposition. The fuel cell with the 13 μm AFL can be operated with stable output over 85 h, whereas a little carbon fiber was observed in the Ni–YSZ anode layer after 130 h operation.

Acknowledgments

The authors gratefully acknowledge the research funding provided by the National Natural Science Foundation of China (21076118, 21176187 and 21173147), Promotive Research Fund for Excellent Young and Middle-aged Scientists of Shandong Province (2010BSB01011), and Tianjin Research Program of Application Foundation and Advanced Technology (11JCZDJC23400).

References

[1] K. Kendall, Int. J. Appl. Ceram. Technol. 7 (2010) 1–9.
[2] M.P. Kevin Kendall, J. Power Sources 71 (1998) 268–270.
[3] V. Lawlor, S. Griesser, G. Buchinger, A.G. Olabi, S. Cordiner, D. Meissner, J. Power Sources 193 (2009) 387–399.
[4] R.J. Gorte, J.M. Vohs, Curr. Opin. Colloid Interface Sci. 14 (2009) 236–244.
[5] M.D. Gross, J.M. Vohs, R.J. Gorte, J. Electrochem. Soc. 154 (2007) B694–B699.
[6] X.-F. Ye, S.R. Wang, Z.R. Wang, L. Xiong, X.F. Sun, T.L. Wen, J. Power Sources 177 (2008) 419–425.
[7] X.-F. Ye, S.R. Wang, Q. Hu, Z.R. Wang, T.L. Wen, Z.Y. Wen, Electrochem. Commun. 11 (2009) 823–826.
[8] F. Zhao, A. Virkar, J. Power Sources 141 (2005) 79–95.
[9] Y.M. Park, H.J. Lee, H.Y. Bae, J.S. Ahn, H. Kim, Int. J. Hydrogen Energy 37 (2012) 4394–4400.
[10] K. Chen, X. Chen, Z. Lü, N. Ai, X. Huang, W. Su, Electrochim. Acta 53 (2008) 7825–7830.
[11] L. Bi, E. Fabbri, E. Traversa, Electrochem. Commun. 16 (2012) 37–40.
[12] T. Suzuki, S. Sugihara, T. Yamaguchi, H. Sumi, K. Hamamoto, Y. Fujishiro, Electrochem. Commun. 13 (2011) 959–962.
[13] X.-F. Ye, S.R. Wang, J. Zhou, F.R. Zeng, H.W. Nie, T.L. Wen, J. Power Sources 196 (2011) 5499–5502.
[14] N. Droushiotis, M.H.D. Othman, U. Doraswami, Z. Wu, G. Kelsall, K. Li, Electrochem. Commun. 11 (2009) 1799–1802.
[15] M.H.D. Othman, N. Droushiotis, Z. Wu, G. Kelsall, K. Li, Adv. Mater. 23 (2011) 2480–2483.
[16] M.H.D. Othman, N. Droushiotis, Z. Wu, G. Kelsall, K. Li, J. Power Sources 205 (2012) 272–280.
[17] M.H.D. Othman, Z. Wu, N. Droushiotis, U. Doraswami, G. Kelsall, K. Li, J. Membr. Sci. 351 (2010) 196–204.
[18] X. Meng, X. Gong, N. Yang, X. Tan, Y. Yin, Z.-F. Ma, J. Power Sources 237 (2013) 277–284.
[19] X. Meng, X. Gong, Y. Yin, N.-T. Yang, X. Tan, Z.-F. Ma, Int. J. Hydrogen Energy (2013).
[20] V. Sariboğa, F. Öksüzömer, Appl. Energy 93 (2012) 707–721.
[21] Y. Lin, Z. Zhan, J. Liu, S. Barnett, Solid State Ionics 176 (2005) 1827–1835.
[22] C. Zuo, S. Zha, M. Liu, M. Hatano, M. Uchiyama, Adv. Mater. 18 (2006) 3318–3320.
[23] C. Jin, C. Yang, F. Chen, J. Membr. Sci. 363 (2010) 250–255.
[24] Y. Leng, S. Chan, S. Jiang, K. Khor, Solid State Ionics 170 (2004) 9–15.
[25] C.W. Tanner, K.Z. Fung, A.V. Virkar, J. Electrochem. Soc. 144 (1997) 21–30.
[26] J.B. Goodenough, Y.-H. Huang, J. Power Sources 173 (2007) 1–10.
[27] K.S. Howe, G.J. Thompson, K. Kendall, J. Power Sources 196 (2011) 1677–1686.
[28] E.W. Park, H. Moon, M.-S. Park, S.H. Hyun, Int. J. Hydrogen Energy 34 (2009) 5537–5545.
[29] O. Costa-Nunes, R.J. Gorte, J.M. Vohs, J. Power Sources 141 (2005) 241–249.
[30] M. Schmal, C.A. Perez, V.T. da Silva, L.F. Padilha, Appl. Catal. A Gen. 375 (2010) 205–212.
[31] A.C. Ferreira, A.M. Ferraria, A.M.B. do Rego, A.P. Gonçalves, A.V. Girão, R. Correia, T.A. Gasche, J.B. Branco, J. Mol. Catal. A Chem. 320 (2010) 47–55.
[32] A. Singh, J.M. Hill, J. Power Sources 214 (2012) 185–194.
[33] J. Fisherii, S. Chuang, Catal. Commun. 10 (2009) 772–776.